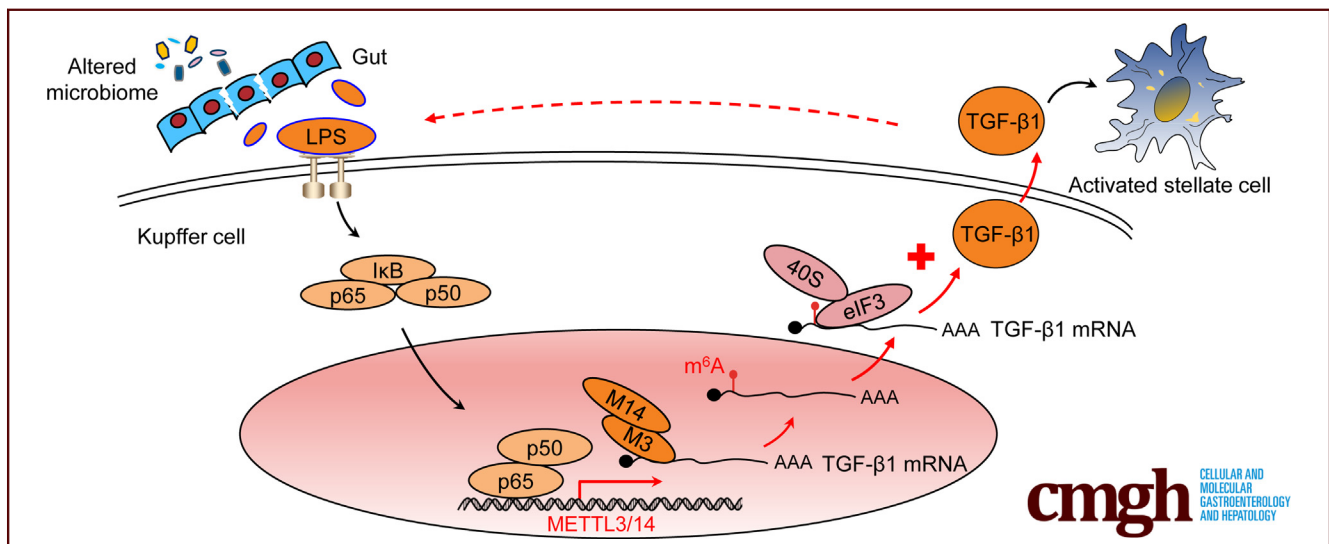


ORIGINAL RESEARCH

METTL3/METTL14 Transactivation and m⁶A-Dependent TGF- β 1 Translation in Activated Kupffer Cells

Yue Feng,^{1,2} Haibo Dong,^{1,2} Bo Sun,^{1,2} Yun Hu,^{1,2} Yang Yang,^{1,2} Yimin Jia,^{1,2} Longfei Jia,⁴ Xiang Zhong,³ and Ruqian Zhao^{1,2}

¹MOE Joint International Research Laboratory of Animal Health & Food Safety, Nanjing Agricultural University, Nanjing, Jiangsu, P. R. China; ²Key Laboratory of Animal Physiology and Biochemistry, College of Veterinary Medicine, Nanjing Agricultural University, Nanjing, Jiangsu, P. R. China; ³College of Animal Science and Technology, Nanjing Agricultural University, Nanjing, Jiangsu, P. R. China; and ⁴Division of Nutritional Sciences, Cornell University, Ithaca, New York



SUMMARY

NF- κ B p65 directly transactivates METTL3/METTL14 genes upon LPS challenge, leading to global m⁶A hypermethylation. Increased m⁶A on the 5'UTR of TGF- β 1 mRNA results in m⁶A-dependent translation in a cap-independent manner, which sheds light on the molecular mechanism of NASH progression.

BACKGROUND AND AIMS: Transforming growth factor β 1 (TGF- β 1) secreted from activated Kupffer cells (KC) promotes the progression of nonalcoholic steatohepatitis (NASH) to liver fibrosis. N⁶-methyladenosine (m⁶A) RNA modification participates in various cell stress responses, yet it remains unknown whether it plays a role in TGF- β 1 upregulation in activated KCs.

METHODS: Western blot, dot blot, and liquid chromatography with tandem mass spectrometry were used to determine the expression of m⁶A methyltransferase, METTL3, and METTL14, as well as global m⁶A modification. RNA-sequencing and m⁶A-seq were employed to screen differentially expressed genes and responsive m⁶A peaks. Nuclear factor κ B (NF- κ B)-mediated METTL3/METTL14 transactivation were validated with

chromatin immunoprecipitation polymerase chain reaction and dual-luciferase reporter system, and the role of m⁶A in TGF- β 1 upregulation was further verified in METTL3/METTL14-deficient KCs and myeloid lineage cell-specific METTL14 knockout mice.

RESULTS: Serum lipopolysaccharide (LPS) concentration is increased in high-fat diet-induced NASH rats. TGF- β 1 upregulation is closely associated with METTL3/METTL14 upregulation and global m⁶A hypermethylation, in both NASH rat liver and LPS-activated KCs. LPS-responsive m⁶A peaks are identified on the 5' untranslated region (UTR) of TGF- β 1 messenger RNA (mRNA). NF- κ B directly transactivates METTL3 and METTL14 genes. LPS-stimulated TGF- β 1 expression is abolished in METTL3/METTL14-deficient KCs and myeloid lineage cell-specific METTL14 knockout mice. Mutation of m⁶A sites on the 5'UTR of TGF- β 1 mRNA blocks LPS-induced increase of luciferase reporter activity.

CONCLUSIONS: NF- κ B acts as transcription factor to transactivate METTL3/METTL14 genes upon LPS challenge, leading to global RNA m⁶A hypermethylation. Increased m⁶A on the 5'UTR of TGF- β 1 mRNA results in m⁶A-dependent translation of TGF- β 1 mRNA in a cap-independent manner. We identify a novel role of m⁶A modification in TGF- β 1 upregulation, which helps to shed light on the molecular mechanism of NASH

progression. (*Cell Mol Gastroenterol Hepatol* 2021;12:839–856; <https://doi.org/10.1016/j.jcmgh.2021.05.007>)

Keywords: NASH; N6-Methyladenosine; TGF- β 1; NF- κ B.

The transition from nonalcoholic steatohepatitis (NASH) to fibrosis is critical in the pathogenesis of hepatocellular carcinoma.¹ Transforming growth factor β 1 (TGF- β 1) is the most potent profibrogenic factor involved in the initiation and maintenance of fibrogenesis in the liver.^{2,3} In high-fat diet (HFD)-induced NASH model, the gut microbial components, such as lipopolysaccharide (LPS), leaks into the circulation due to disruption of gut barrier functions and transfers to the liver via hepatic portal vein.^{4–6} Kupffer cells (KCs), the liver-resident macrophages, are activated by LPS exposure and secrete TGF- β 1 to stimulate hepatic stellate cells transformation and extracellular matrix components production, leading to fibrosis. Therefore, TGF- β 1 secreted from activated KCs serves as a critical mediator in NASH to fibrosis progression.

N6-methyladenosine (m⁶A) is the most abundant and dynamically regulated modification throughout the transcriptome, which affects RNA splicing, translation, and stability.⁷ The formation, elimination and function of m⁶A are determined by “writers,” “erasers,” and “readers.”⁸ Numerous studies indicate that m⁶A plays a critical role in immune and inflammatory responses.⁹ For example, m⁶A participates in Th cell differentiation and proliferation,¹⁰ dendritic cells maturation,¹¹ and LPS-induced inflammatory responses in dental pulp cells.¹² Recently, 2 independent groups reported controversial role of m⁶A in HCC progression. Ma et al¹³ reported that m⁶A modification is decreased in HCC samples and upregulation of methyltransferase METTL14 suppresses HCC metastasis, whereas Chen et al¹⁴ found that m⁶A modification is elevated in HCC samples and upregulation of methyltransferase METTL3 contributes to HCC progression. Both studies used liver samples containing different cell types, as well as hepatocyte-derived carcinoma cell lines such as HepG2 and Huh-7. The discrepancy between the 2 studies indicates complex role of m⁶A and its regulatory enzymes in HCC progression, which is likely dependent on the stage of HCC or the type of cells involved in the progression. Until now, it remains unknown whether m⁶A is involved in KCs activation and TGF- β 1 expression.

In this study, we first detected significant upregulation of METTL3/METTL14 and global RNA m⁶A hypermethylation in the liver of HFD-induced NASH rat model and LPS-activated KC lines. We found that nuclear factor κ B (NF- κ B) p65 directly transactivates both METTL3 and METTL14 genes, thereby leading to global RNA m⁶A hypermethylation. METTL3/METTL14 knockdown in KCs decreases m⁶A and abolishes LPS-induced TGF- β 1 secretion in vitro. Myeloid lineage cell-specific METTL14 knockout mice show diminished TGF- β 1 response to LPS or CCl₄ challenge in vivo. Furthermore, LPS increases m⁶A modification on the 5' untranslated region (UTR) of TGF- β 1 messenger RNA (mRNA), leading to m⁶A-dependent translation of TGF- β 1 mRNA in a

cap-independent manner. Our findings extend the current knowledge on the role of m⁶A in TGF- β 1 expression in activated KCs that contributes to fibrosis progression in NASH.

Results


NASH Is Associated With Increased Global m⁶A Modification

We first established a NASH model in rats by feeding HFD for 16 weeks. HFD-fed rats show significantly elevated serum level of LPS (Figure 1A) and augmented hepatic expression of inflammatory cytokines (Figure 1B and C). TGF- β 1 protein concentration increased about 2-fold in HFD-fed rat liver (Figure 1C). These changes combined with significant plasma aspartate aminotransferase and alanine aminotransferase activity (Figure 1D), as well as elevated hepatic NF- κ B pathway activation (Figure 1E), indicate inflammation and hepatocyte injury, the hallmarks of NASH. Sirius Red in saturated carbazotic acid staining and Masson trichrome staining show more collagen fibers in the liver of HFD rats (Figure 1F and G), indicating a progressive NASH and an early stage of liver fibrosis. This is also supported by significantly increased protein content of extracellular matrix components such as collagen-I and α smooth muscle actin in the liver (Figure 1H and I). Concurrently, global m⁶A modification (Figure 1J and K) was significantly more enriched in the liver of HFD-fed rats, which was associated with upregulated methyltransferases, METTL3 and METTL14, and downregulated demethylase fat mass and obesity-associated protein (Figure 1L).

LPS-Activated KCs Exhibit m⁶A Hypermethylation

To establish a cell-specific link between KC activation and m⁶A hypermethylation, we treated KCs with LPS at 1 ng/mL that is equivalent to the plasma LPS level (3 EU/mL) in HFD-fed rats (Figure 1A). KC activation was confirmed by elevated interleukin (IL)-6 and TGF- β 1 protein levels (Figure 2A), immunofluorescence staining of TGF- β 1 (Figure 2B), and Kyoto Encyclopedia of Genes and Genomes pathway analysis of RNA-sequencing database (Figure 2C). Both RNA-sequencing and quantitative polymerase chain reaction (qPCR) indicate significant upregulation of IL-1 β , IL-6, tumor necrosis factor α (TNF- α), and TGF- β 1, but not

Abbreviations used in this paper: ChIP, chromatin immunoprecipitation; cKO, conditional knockout; DC, dendritic cell; HFD, high-fat diet; IL, interleukin; KC, Kupffer cell; KO, knockout; LPS, lipopolysaccharide; m⁶A, N6-methyladenosine; MeRIP-seq, methylated RNA immunoprecipitation sequencing; mRNA, messenger RNA; NASH, nonalcoholic steatohepatitis; NF- κ B, nuclear factor κ B; PCR, polymerase chain reaction; qPCR, quantitative polymerase chain reaction; SELECT, single-base elongation- and ligation-based qPCR amplification method; siRNA, small interfering RNA; TGF- β 1, transforming growth factor β 1; TNF- α , tumor necrosis factor alpha; UTR, untranslated region; WT, wild-type.

 Most current article

© 2021 The Authors. Published by Elsevier Inc. on behalf of the AGA Institute. This is an open access article under the CC BY-NC-ND license (<http://creativecommons.org/licenses/by-nc-nd/4.0/>).

2352-345X

<https://doi.org/10.1016/j.jcmgh.2021.05.007>

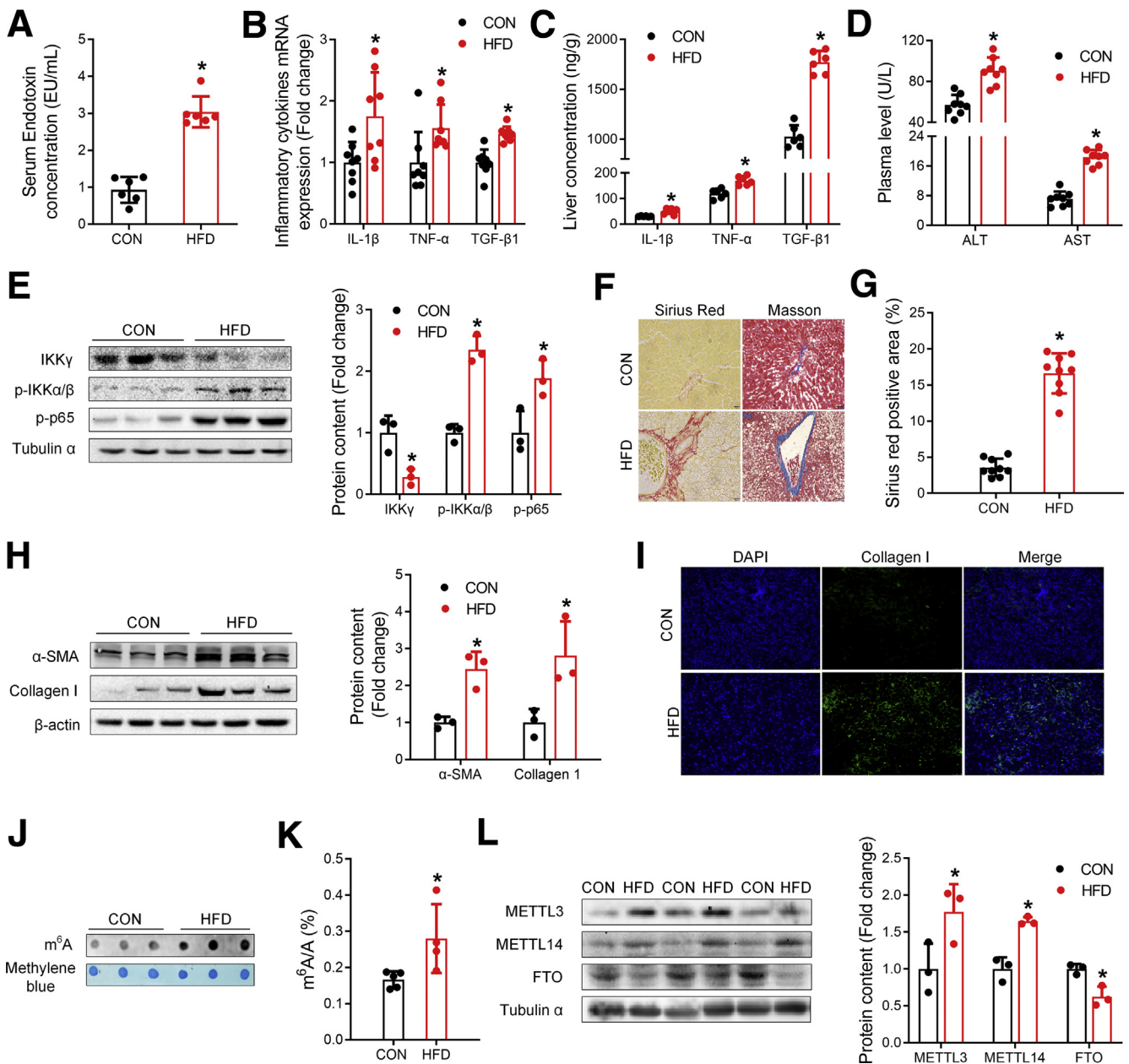


Figure 1. Global m⁶A modification level is increased in the HFD rat model. (A) Serum endotoxin concentration was measured by Endotoxin Test Kit; $n = 6$; mean \pm SD; Student's t test; $*P < .05$. (B, C) (Liver inflammatory cytokines mRNA expression and concentrations were measured by qPCR and enzyme-linked immunosorbent assay; $n = 6$; mean \pm SD; Student's t test; $*P < .05$. (D) Aspartate aminotransferase (AST) and alanine aminotransferase (ALT) activities in plasma were measured by biochemical automatic analyzer; $n = 6$; mean \pm SD; Student's t test; $*P < .05$. (E) Inflammatory NF- κ B pathway-related protein content was detected by Western blot; $n = 3$; mean \pm SD; Student's t test; $*P < .05$. (F) Sirius Red (red area) and Masson (blue area) staining in rat liver during HFD administration; $n = 3$. (G) Percentage in area of positive staining for Sirius Red. Positive area was quantified using ImageJ software; $n = 3$; mean \pm SD; Student's t test; $*P < .05$. (H) Liver fibrosis-related proteins content were measured by Western blot; $n = 3$; mean \pm SD; Student's t test; $*P < .05$. (I) Collagen I expression was assessed by immunofluorescence. Nucleus was stained with DAPI; magnification = 200 \times ; $n = 3$. (J, K) Global m⁶A level of rat liver mRNA was detected by dot blot and high-performance liquid chromatography with tandem mass spectrometry; $n = 3$; mean \pm SD; Student's t test; $*P < .05$. (L) METTL3, METTL14, and fat mass and obesity-associated protein (FTO) protein content in rat liver during HFD treatment and statistics; $n = 6$; mean \pm SD; Student's t test; $*P < .05$. α -SMA, α -smooth muscle actin; CON, control diet with 10% of energy from fat.

TGF- β 2 or TGF- β 3, in LPS-activated KCs (Figure 2D–F). KC activation is also linked with significant m⁶A hypermethylation, as shown in dot-blot and high-performance

liquid chromatography with tandem mass spectrometry analyses (Figure 2G and H). In line with m⁶A hypermethylation, a significant upregulation of METTL3 and

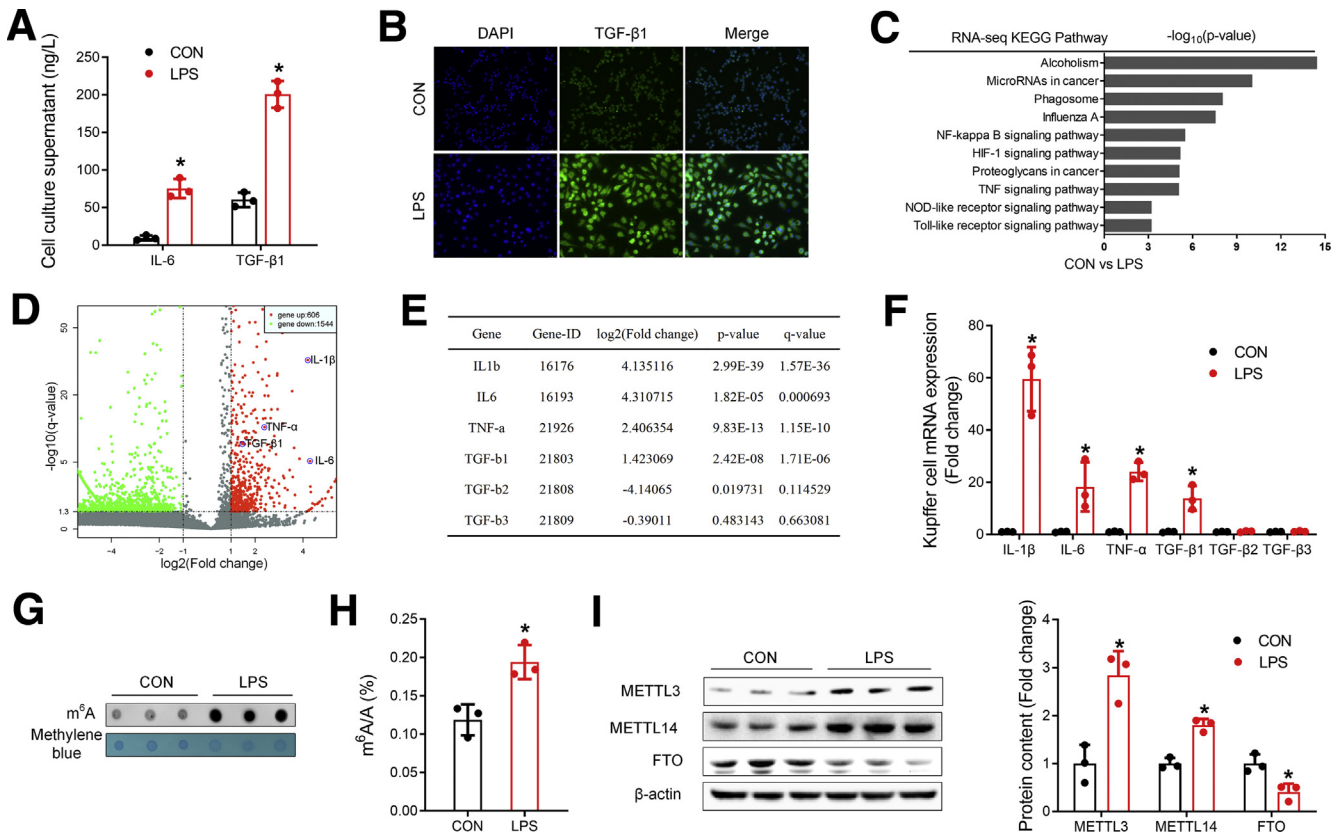


Figure 2. Global m⁶A modification level is increased in activated KCs. (A) IL-6 and TGF- β 1 content in KC supernatant were measured by enzyme-linked immunosorbent assay; $n = 6$; mean \pm SD; Student's t test; $*P < .05$. (B) TGF- β 1 expression was assessed by immunofluorescence. Nucleus was stained with DAPI; magnification = 40 \times ; $n = 3$. (C) RNA-sequencing Kyoto Encyclopedia of Genes and Genomes (KEGG) enrichment analysis of transcripts expression compared CON with LPS; $n = 2$. (D–F) RNA-sequencing ($n = 2$) and qPCR ($n = 3$) show that compared with TGF- β 2 and TGF- β 3, IL-1 β /IL-6/TNF- α /TGF- β 1 were significantly upregulated in LPS group; mean \pm SD; Student's t test; $*P < .05$. (G, H) Global m⁶A level of activated KCs was detected by dot blot and high-performance liquid chromatography with tandem mass spectrometry; $n = 3$; mean \pm SD; Student's t test; $*P < .05$. I, METTL3, METTL14, and fat mass and obesity-associated protein (FTO) protein content in activated KCs during LPS treatment and statistics; $n = 3$; mean \pm SD; Student's t test; $*P < .05$.

METTL14, together with a significant downregulation of fat mass and obesity-associated protein, were determined in LPS-treated KCs (Figure 2I).

NF- κ B p65 Directly Activates the Transcription of METTL3 and METTL14 Genes

To understand whether NF- κ B is involved in METTL3/METTL14 upregulation in LPS-activated KCs, we treated KCs with LPS with or without NF- κ B p65 inhibitor JSH-23. JSH-23 completely reversed LPS-induced upregulation of both METTL3 and METTL14 at mRNA and protein level (Figure 3A–D). To validate whether NF- κ B p65 directly transactivate METTL3/METTL14, we used ChIP-qPCR and found that LPS significantly increased binding of p65 on predicted binding sites (Figure 3E) of both METTL3/METTL14 gene promoters (Figure 3F). Further, dual-luciferase reporter system confirmed the functionality of these binding sites. Deletion of these binding sites in METTL3 and METTL14 promoters blocked LPS-induced activation

of METTL3 and METTL14 genes promoters (Figure 3G–I). These results indicate a role of NF- κ B p65 in direct transactivation of METTL3 and METTL14 genes upon LPS challenge.

LPS-Responsive m⁶A Sites Are Identified on the 5'UTR of TGF- β 1 mRNA

To elaborate the locus-specific distribution of m⁶A hypermethylation in LPS-activated KCs, we employed methylated RNA immunoprecipitation sequencing (MeRIP-seq), and identified 2859 differential m⁶A peaks, with 1273 upregulated and 1586 downregulated upon LPS treatment. GGACU represents highly enriched sequence motif for m⁶A modification (Figure 4A), and m⁶A peaks are concentrated near the translation start and stop codons (Figure 4B).

Interestingly, m⁶A peaks on the 5'UTR showed the greatest response, which is increased from 4.57% in the group fed a control diet with 10% of energy from fat to 7.05% in LPS (Figure 4C). The LPS-responsive m⁶A peaks are clustered in immune and inflammatory responses in

Gene Ontology analysis (Figure 4D), and enriched specifically in NF- κ B and TNF signaling pathways in Kyoto Encyclopedia of Genes and Genomes pathway analysis (Figure 4E). Further data mining of the MeRIP-seq database leads to the discovery of TGF- β 1, as the m⁶A peaks on its 5'UTR are LPS-responsive (Figure 5A). The LPS responsiveness of these m⁶A peaks on the 5'UTR of TGF- β 1 mRNA was further confirmed by MeRIP-qPCR (Figure 5B). Such LPS response in m⁶A modification appears to be locus specific, as TNF- α mRNA showed no significant change in m⁶A modification (Figure 5C and D), and m⁶A modification was not detected in either IL-1 β or IL-6 mRNAs. In line with a previous report on dendritic and T cells,¹⁰ Socs3 also showed significant increase in m⁶A peaks (Figure 5E and F) in response to LPS challenge.

We went on to predict the specific m⁶A sites on TGF- β 1 5'UTR (25687587-25687822 nt) with a sequence-based m⁶A modification site predictor. We identified 4 putative motifs, among which motif 4 reached a score of high confidence (X site, Figure 5G). We verified the motif 4 with the single-base elongation- and ligation-based qPCR amplification method (SELECT) method that exploits the ability of m⁶A to hinder the single-base elongation activity of DNA polymerases and the nick ligation efficiency of ligases.¹⁵ Cycle threshold number was significantly increased at X site (Figure 5H), but not at the negative control site (N site, Figure 5I), indicating increased m⁶A modification on motif 4 of TGF- β 1 5'UTR in LPS-treated KCs.

METTL3/METTL14 Knockdown Abolishes LPS-Induced KC Activation in an m⁶A Dependent Manner

To understand the role of m⁶A modification in LPS-induced KC activation, we used small interfering RNAs (siRNAs) to knock down both METTL3 and METTL14. METTL3/METTL14 knockdown significantly reduced the basal expression and completely abolished the LPS-induced METTL3 and METTL14 upregulation (Figure 6A). METTL3/METTL14 knockdown significantly abolished LPS-induced m⁶A hypermethylation (Figure 6B) and KC activation, indicated by significantly diminished LPS response in TGF- β 1 expression (Figure 6C) and secretion (Figure 6D), suppressed immunofluorescent staining of CD68 (Figure 6E) and TGF- β 1 (Figure 6F). Accordingly, METTL3 overexpression significantly enhanced the basal expression of TGF- β 1 in KCs (Figure 6G). Further, stellate cells (JS1) were cultured with conditioned medium from LPS-activated wild-type (WT) or METTL3/METTL14 knockdown KCs. The conditioned medium from KCs lacking METTL3/METTL14 induced significantly blunted collagen I response in JS1 cells (Figure 6H). However, METTL3/METTL14 knockdown did not affect LPS-induced NF- κ B activation, as the phosphorylated p65 protein content was not altered (Figure 6C). These data further confirm that METTL3 and METTL14 are downstream of NF- κ B signaling and are indispensable for LPS-induced KC activation and TGF- β 1 expression.

METTL14 Conditional Knockout Blocks LPS- and CCl4-Induced TGF- β 1 Production in Mouse Primary KC

To investigate the role of m⁶A in TGF- β 1 regulation in vivo, we injected WT and METTL14 conditional knockout (cKO) mice with LPS and CCl₄, respectively. Lack of METTL14 significantly inhibited infiltration of immune cells (Figure 7A) and completely abolished TGF- β 1 response in isolated primary KCs (Figure 7B) and LPS-treated mouse liver (Figure 7C). Meanwhile, Lack of METTL14 significantly inhibited m⁶A modification on the TGF- β 1 mRNA 5'UTR motif 4 (Figure 7D and E). METTL14 deficiency also protected mice from CCl₄-induced hepatic fibrosis, indicated by less collagen fibers in Sirius Red staining (Figure 7F) and attenuated TGF- β 1 response both in mouse liver (Figure 7G) and isolated primary KCs (Figure 7H). SELECT analysis supports the notion that lack of METTL14 abolishes response of m⁶A motif 4 on the 5'UTR of TGF- β 1 transcript (Figure 7I and J).

m⁶A on the 5'UTR of TGF- β 1 mRNA Promotes Cap-Independent Translation

We first tested whether m⁶A sites on the 5'UTR of TGF- β 1 mRNA affect mRNA stability and found no difference in the lifetime of TGF- β 1 mRNA between control and LPS-treated KCs (Figure 8A). We then tested whether these m⁶A sites promote mRNA translation through YTHDF3/YTHDF1-dependent pathway. YTHDF3 was significantly increased upon LPS treatment, yet YTHDF3 siRNA failed to abolish LPS-induced increase of either YTHDF3 or TGF- β 1 (Figure 8B and C). YTHDF1 was not responsive to LPS, yet a slight but significant increase of YTHDF1 was detected in YTHDF1 knockdown KCs in response to LPS challenge. Also, YTHDF1 knockdown failed to abolish LPS-induced TGF- β 1 expression in KCs (Figure 8D and E). These data indicate that LPS-induced TGF- β 1 expression is not due to increased mRNA stability or YTHDF1/YTHDF3-dependent translation efficiency.

We further tested whether TGF- β 1 translation is dependent on the cap-binding factor eIF4E. We knocked down the eIF4E (Figure 8F) and found that LPS-induced TGF- β 1 upregulation is not dependent on eIF4E (Figure 9A-C). We conducted luciferase reporter assays with plasmids (Figure 9D) carrying a wild-type TGF- β 1 5'UTR (WT) and 4 mutants in which each of the 4 m⁶A motifs on the 5'UTR of TGF- β 1 mRNA was respectively mutated (MUT 1-4). The mutation of the motif 4 (MUT4) abolished LPS-induced increase in luciferase activity of TGF- β 1 5'UTR (Figure 9E), suggesting that m⁶A modification on this specific site is indispensable for TGF- β 1 upregulation in LPS-activated KCs. To validate m⁶A-mediated cap-independent translation of TGF- β 1, a translation experiment was conducted using 6 types of in vitro transcribed reporter mRNAs with 3 different caps: noncap, nonfunctional (A_{ppp}G) cap, or normal cap (m⁷G), each with wild-type (normal, A) or mutant (MUT to T) m⁶A site of TGF- β 1 5'UTR and full-length firefly luciferase (Figure 9F). The results showed that the reporter mRNAs carrying noncap and

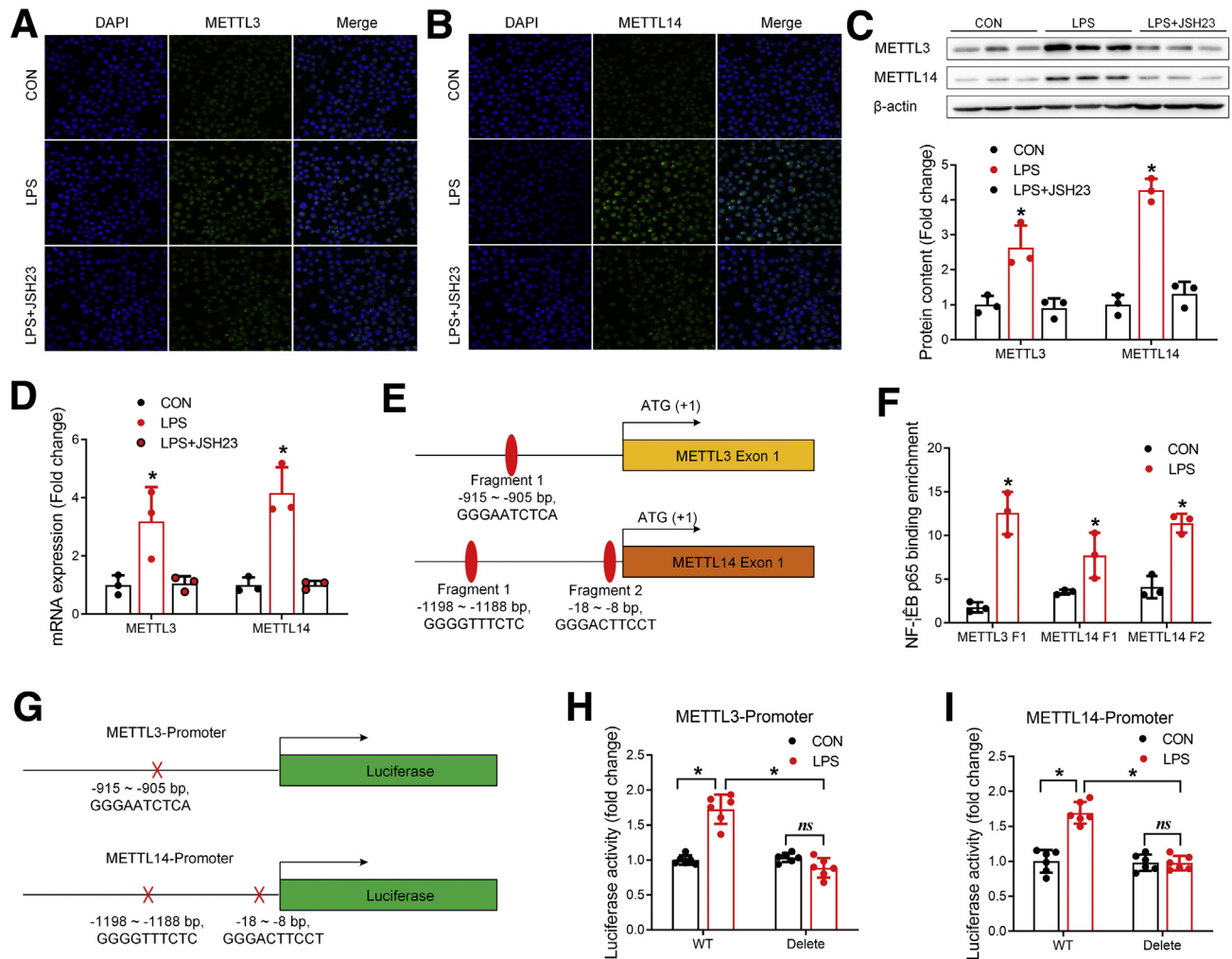


Figure 3. NF- κ B p65 directly activates the transcription of METTL3 and METTL14 genes. (A–D) Immunofluorescence, Western blot, and qPCR were used to detect the METTL3/METTL14 protein content and mRNA expression after treatment with NF- κ B inhibitor JSH23; DAPI was used for nuclear staining; cells analyzed with a confocal laser scanning microscope (40 \times magnification) with Z-scan analysis; $n = 3$; mean \pm SD; 2-way analysis of variance followed by Tukey's test for multiple comparisons; $*P < .05$. (E) Schematic representation of transcription factor binding promoter of METTL3/METTL14. (F) ChIP-PCR assay was used to measure the binding of NF- κ B on METTL3/METTL14 promoter in KCs with or without treatment of LPS; $n = 3$; mean \pm SD; Student's t test; $*P < .05$. METTL3 F1, METTL14 F1, and METTL14 F2 mean METTL3 fragment 1, METTL14 fragment 1, and METTL14 fragment 2, respectively. (G–I) Dual-luciferase activity of normal and binding site-deleted METTL3/METTL14 promoter by LPS treatment in KCs; $n = 3$; mean \pm SD; 2-way analysis of variance followed by Tukey's test for multiple comparisons; $*P < .05$.

nonfunctional cap had no translation activity when the m⁶A site of TGF- β 1 5'UTR was mutated, while the reporter mRNAs carrying normal cap (m⁷G) with mutant m⁶A site showed reduced translation efficiency (Figure 9G). These results demonstrate m⁶A-dependent translation in TGF- β 1 expression.

In summary, we demonstrate that m⁶A modification is essential for TGF- β 1 posttranscriptional regulation in the process of NASH to liver fibrosis. The classic inflammatory NF- κ B pathway hijacks the m⁶A methyltransferases METTL3 and METTL14 to empower cap-independent translation of TGF- β 1, thus aggravating TGF- β 1-mediated stellate cell activation to promote the process of NASH to liver fibrosis transition (Figure 10).

Discussion

TGF- β 1 is a master profibrogenic cytokine and a promising target for the treatment of fibrosis.¹⁶ TGF- β 1 expression is regulated at both transcription and translation levels, through signaling pathways involving p38 MAPK, ERK, and JNK, as well as Rho GTPase, PI3K, Akt, and mammalian target of rapamycin.¹⁷ Here, we provide evidences that mRNA m⁶A modification is critical in LPS-induced TGF- β 1 upregulation in activated KCs, adding another layer of regulation in TGF- β 1 expression.

A number of studies suggest a role of m⁶A in various cellular stress responses, such as heat shock response,^{18,19} ultraviolet-induced DNA damage,²⁰ oxidative stress,²¹ and

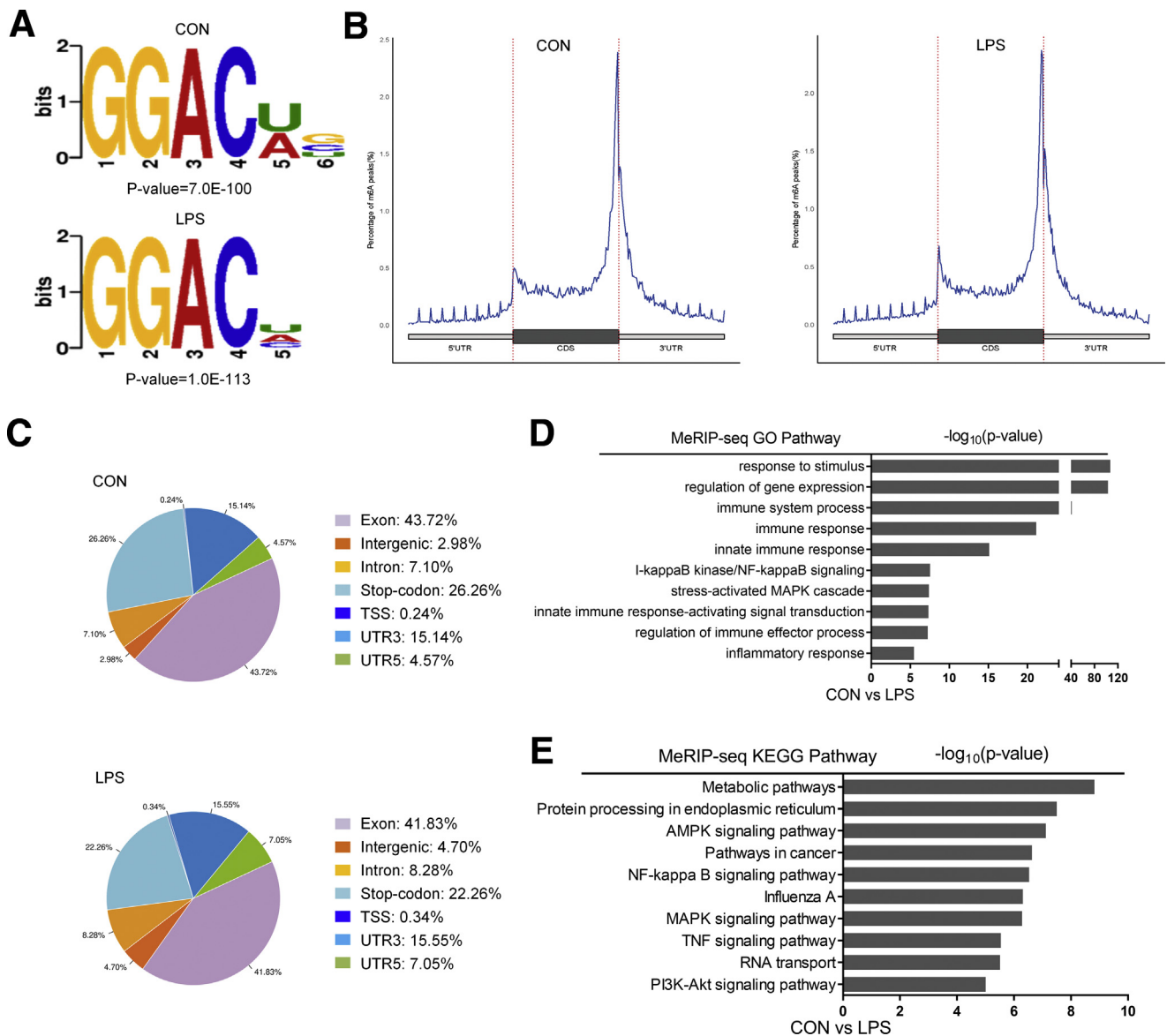


Figure 4. m⁶A modification compared CON with LPS in KCs by MeRIP-seq. (A) Sequence logo representing consensus motif of m⁶A sites in LPS-treatment peaks by MeRIP-seq. (B) m⁶A peak distribution in CDS, 5'UTR, 3'UTR region by MeRIP-seq. (C) Pie chart presenting fractions of m⁶A peaks in different transcript segments. (D, E) Gene Ontology (GO) and Kyoto Encyclopedia of Genes and Genomes (KEGG) enrichment analysis in the biological process and signaling pathway category of transcripts bearing m⁶A modification. MeRIP-seq data are from 1 representative of 2 independent experiments.

inflammatory and immune responses.¹¹ Nevertheless, mechanisms by which m⁶A exerts its regulatory function are widely varied. Three distinct mechanisms are suggested. First, m⁶A regulates RNA stability through its reader proteins YTHDF2 and IGF2BP1–3.^{22,23} Second, m⁶A affects mRNA translation by promoting ribosome loading through m⁶A reader proteins YTHDF3 and YTHDF1 interacting with ribosomal 40S/60S subunits.^{24,25} Third, m⁶A located in the 5'UTR promotes cap-independent translation in heat shock response.^{18,19} We tested all the 3 mechanisms in the present study. The first 2 mechanisms seem unlikely, as TGF- β 1 mRNA decay did not differ between groups fed a control diet with 10% of energy from fat and LPS-treated cells, and knockdown of YTHDF3 and YTHDF1

failed to abolish LPS-induced TGF- β 1 production in KCs. Our results support the third mechanism, as we found that that an m⁶A motif in 5'UTR of TGF- β 1 mRNA mediates TGF- β 1 upregulation in LPS-activated KCs in a cap-independent manner. Similar to the heat shock response, a massive release of cytokines occurs within a short time during inflammatory response, and the immune cells are unable to accomplish the goal merely from de novo gene transcription.^{26–28} This m⁶A-mediated translation machinery is essential for TGF- β 1 production in both LPS-activated KC cell line and primary KC isolated from LPS- or CCl₄-challenged mice. Moreover, mice lacking METTL14 in myeloid lineage cells are protected from CCl₄-induced hepatic fibrosis. These findings suggest an

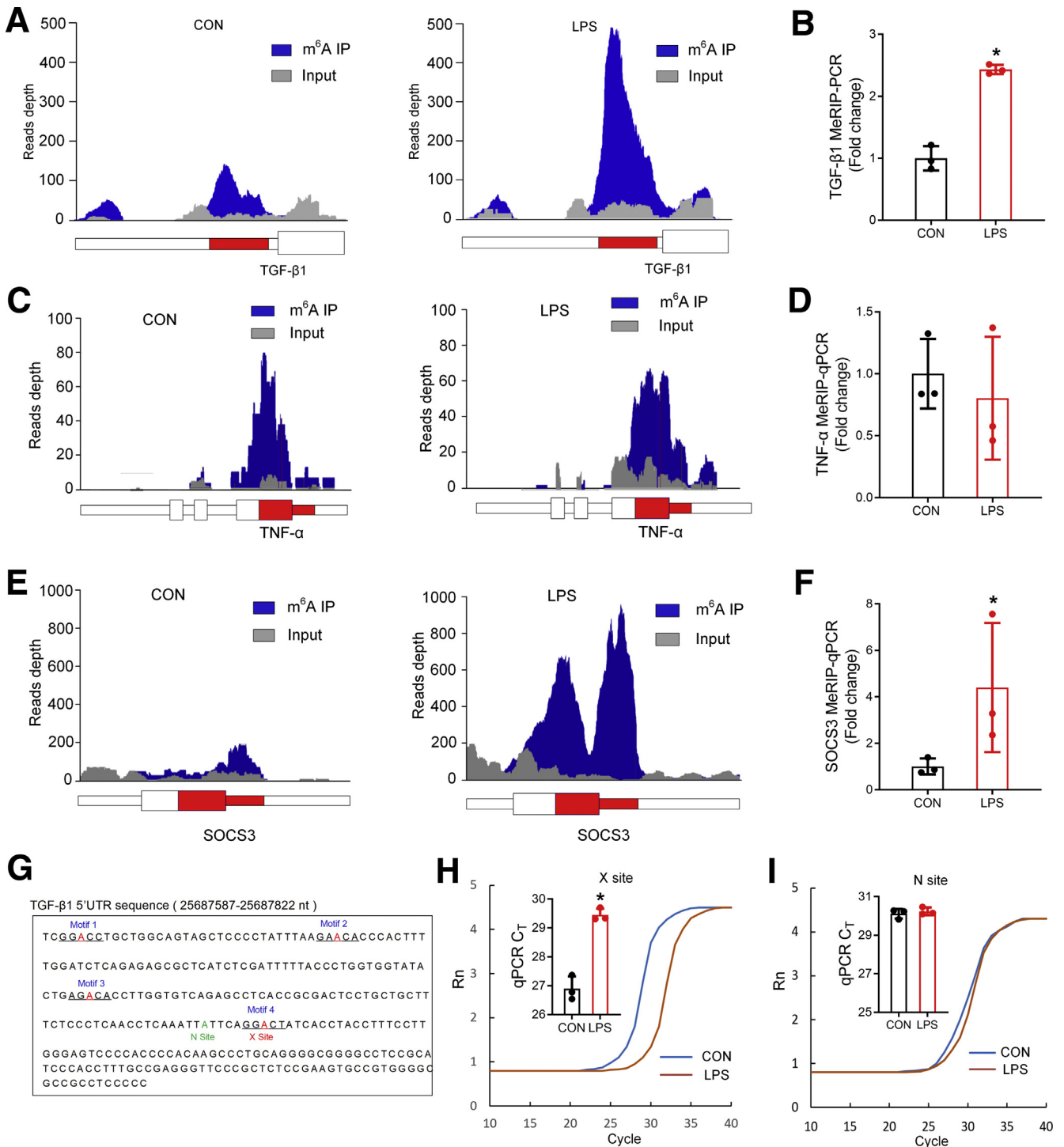


Figure 5. The 5'UTR of TGF- β 1 mRNA is m⁶A hypermethylated in LPS-activated KCs. (A) m⁶A peak marked in red is increased in the 5'UTR of TGF- β 1 gene from m⁶A-seq data in the LPS group. Coverage of m⁶A immunoprecipitation (IP) and control reads (Input) are indicated in blue and gray, respectively. (B) MeRIP-PCR was performed to detect the m⁶A abundance of TGF- β 1 in LPS-treated cells; n = 3; mean \pm SD; Student's *t* test; **P* < .05. (C) TNF- α gene was used as a negative control for MeRIP-seq. The m⁶A peak marked in red is enriched in TNF- α gene last exon and 3'UTR and there is no change when treated with LPS. Coverage of m⁶A IP and control reads (Input) are indicated in blue and gray, respectively. (D) MeRIP-PCR was performed to detect the m⁶A abundance of TNF- α in LPS-treated cells; n = 3; mean \pm SD; Student's *t* test; **P* < .05. (E) The SOCS3 gene was used as a positive control for MeRIP-seq. m⁶A peak marked in red is enriched in the SOCS3 gene last exon and the 3'UTR and is increased when treated with LPS. Coverage of m⁶A IP and control reads (Input) is indicated in blue and gray, respectively. (F) MeRIP-PCR was performed to detect the m⁶A abundance of SOCS3 in LPS-treated cells; n = 3; mean \pm SD; Student's *t* test; **P* < .05. (G) The m⁶A site was predicted in a sequence-based m⁶A modification site predictor for the TGF- β 1 5'UTR 25687587–25687822 nt sequence. The RRACU-compliant motif was named motif 1–4. A high confidence site A was obtained and this motif named motif 4, and this A was named the X site. The nonmodification A was named the N site. (H, I) Validation of m⁶A modification in TGF- β 1 using SELECT. X site was predicted by SRAMP and N site was negative control; n = 3; mean \pm SD; Student's *t* test; **P* < .05. MeRIP-seq data are from 1 representative of 2 independent experiments.

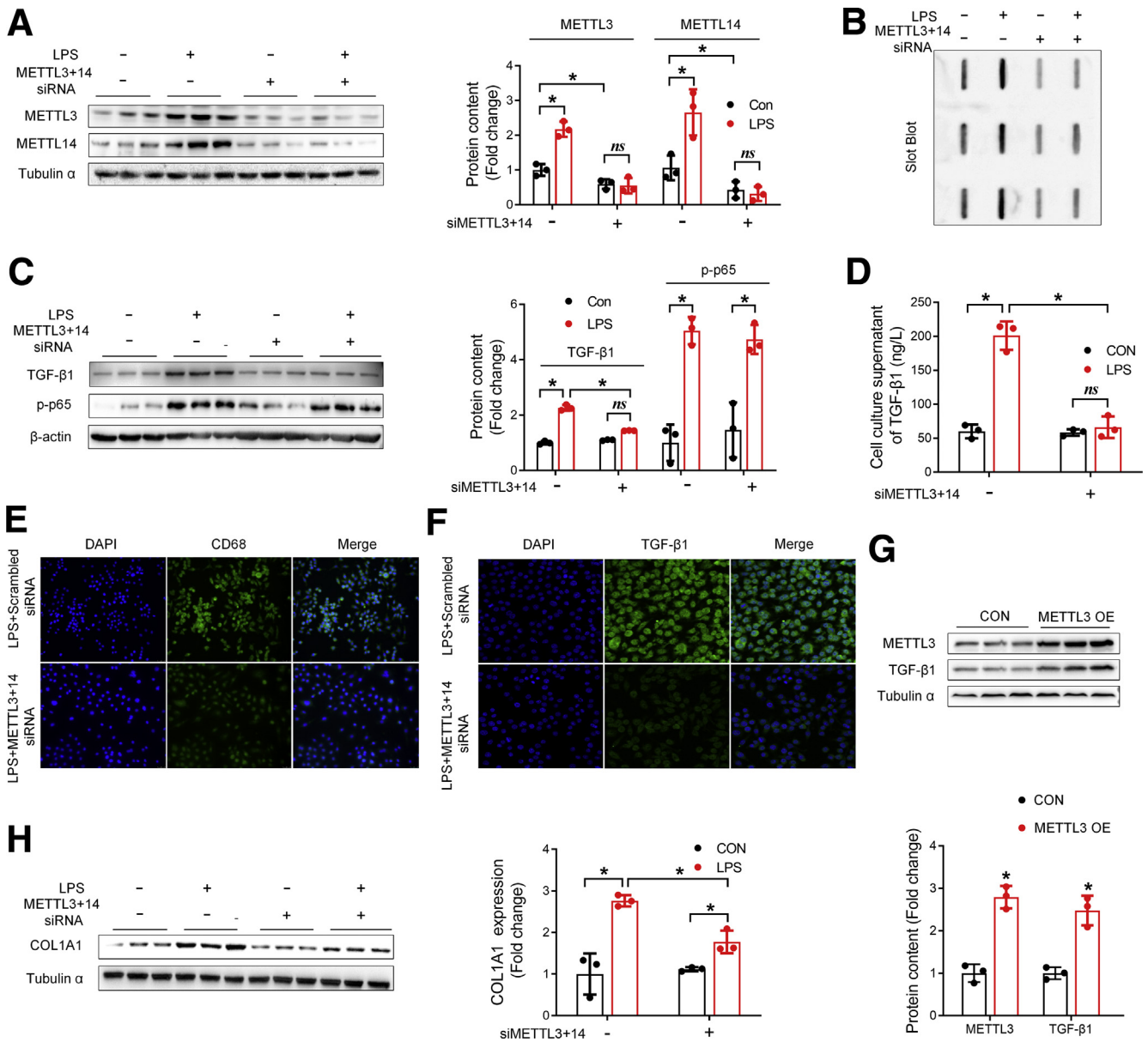


Figure 6. METTL3/METTL14 promote TGF- β 1 translation in an m⁶A catalytic activity-dependent manner. (A) Protein expression of METTL3/METTL14 in METTL3/METTL14 knockdown KCs; $n = 3$; mean \pm SD; 2-way analysis of variance followed by Tukey's test for multiple comparisons; $*P < .05$. (B) m⁶A modification was assessed by slot blot; $n = 6$. (C) Western blot was performed to detect TGF- β 1 and phosphorylated p65 protein content in METTL3/METTL14 knockdown cells; $n = 3$; mean \pm SD; 2-way analysis of variance followed by Tukey's test for multiple comparisons; $*P < .05$. (D) TGF- β 1 content in KC supernatant was measured by enzyme-linked immunosorbent assay kit; $n = 3$; mean \pm SD; 2-way analysis of variance followed by Tukey's test for multiple comparisons; $*P < .05$. (E, F) Protein content of CD68 and TGF- β 1 were detected by immunofluorescence. DAPI was used for nuclear staining. Cells analyzed with a confocal laser scanning microscope (40 \times magnification) with Z-scan analysis. (G) Protein expression of TGF- β 1 in METTL3 overexpression KCs; $n = 3$; mean \pm SD; Student's t test; $*P < .05$. (H) Stellate cells (JS1) were cultured with conditioned medium from LPS-activated WT or METTL3/METTL14 knockdown KCs. $n = 3$; mean \pm SD; 2-way analysis of variance followed by Tukey's test for multiple comparisons; $*P < .05$.

indispensable role of m⁶A and its methyltransferases in fibrosis progression in NASH.

Studies regarding the transcriptional regulation of Mettl3/Mettl14 are relatively scarce. Based on the observation that p65 inhibitor abolishes LPS-induced upregulation of both Mettl3 and Mettl14, we come up with a hypothesis that

p65 may directly transactivate Mettl3 and Mettl14. Data mining from a published ChIP-seencing database GSM1645118²⁹ suggests putative p65 binding sites located about 2 kb upstream of the transcription start site of both METTL3 and METTL14 genes. Further in silico analysis using JARSPER online database identifies 2 putative p65

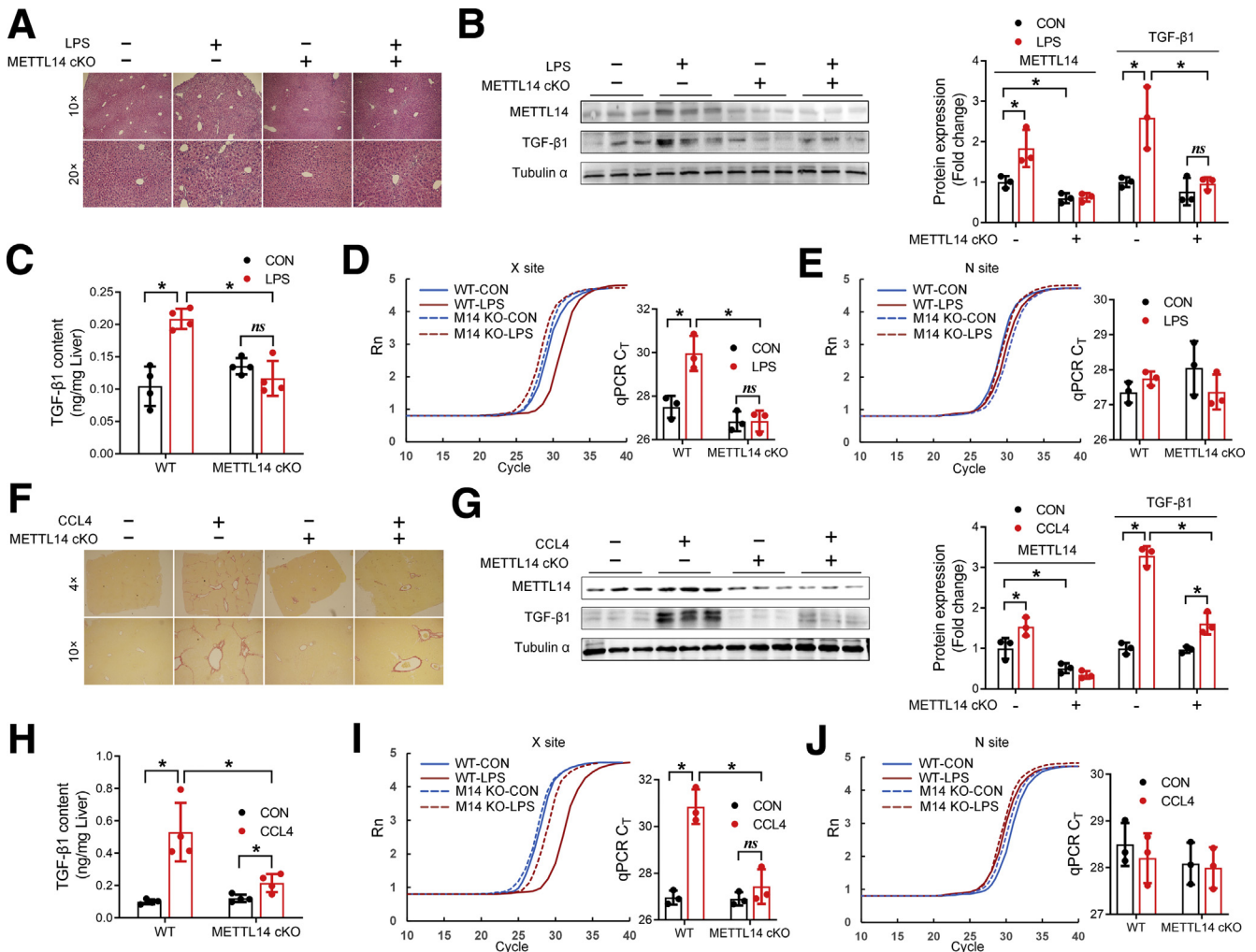


Figure 7. METTL14 cKO blocks LPS-induced TGF- β 1 upregulation. (A) Hematoxylin and eosin staining in METTL14 cKO mice liver when LPS administration; $n = 3$. (B) Primary KCs was isolated from treatment with or without LPS in METTL14 cKO and WT mice, METTL14 and TGF- β 1 expression were measured by Western blot; $n = 3$; mean \pm SD; 2-way analysis of variance followed by Tukey's test for multiple comparisons; $*P < .05$. (C) TGF- β 1 concentrations in the liver was measured by enzyme-linked immunosorbent assay kit; $n = 4$; mean \pm SD; 2-way analysis of variance followed by Tukey's test for multiple comparisons; $*P < .05$. (D, E) Validation of m⁶A modification in TGF- β 1 using SELECT when treatment with LPS in METTL14 cKO mice; $n = 3$; mean \pm SD; Student's t test; $*P < .05$. (F) Sirius Red staining in METTL14 cKO mice liver when CCL4 administration; $n = 3$. (G) Primary KC METTL14 and TGF- β 1 expression were detected by Western blot; $n = 3$; mean \pm SD; 2-way analysis of variance followed by Tukey's test for multiple comparisons; $*P < .05$. (H) TGF- β 1 concentrations in the liver was measured by enzyme-linked immunosorbent assay kit; $n = 4$; mean \pm SD; 2-way analysis of variance followed by Tukey's test for multiple comparisons; $*P < .05$. (I, J) m⁶A modification in TGF- β 1 was detected by SELECT in CCL4-treated METTL14 cKO mice; $n = 3$; mean \pm SD; 2-way analysis of variance followed by Tukey's test for multiple comparisons; $*P < .05$.

binding sites for Mettl3 and 1 for Mettl14. These binding sites were then functionally validated using ChIP assay and promoter activity analysis with luciferase reporter systems. Our results provide strong evidence that NF- κ B p65 binds directly to the promoter of METTL3 and METTL14 genes in KCs to activate their transcription upon LPS stimulation. However, our findings contradict previous publications in which mettl3 acts upstream TLR4/NF- κ B pathway in dendritic cells (DCs)¹¹ and human dental pulp cells.¹² The discrepancy may be explained by differences in cell types (DCs/dental pulp cells vs KCs), or the dose and duration of LPS treatment (100 ng/mL for DCs, 24 hours vs 1 μ g/mL for KCs, 12 hours).

In LPS-induced cytokine cascade or "cytokine storm," proinflammatory factors, such as IL-1 β , IL-6, and TNF- α , can bind again to TLR2/4 to further activate the NF- κ B pathway, thus forming a positive feedback loop. If m⁶A is involved in this cascade, knockdown of METTL3/METTL14 would alleviate, to some extent, LPS-induced activation of NF- κ B pathway. However, this was not the case in the present study. METTL3/METTL14 knockdown abolished LPS-induced TGF- β 1 activation, without affecting NF- κ B activation in KCs. This result confirms that NF- κ B is upstream of METTL3/METTL14, and implicates that the proinflammatory factors may not subject to m⁶A-mediated gene

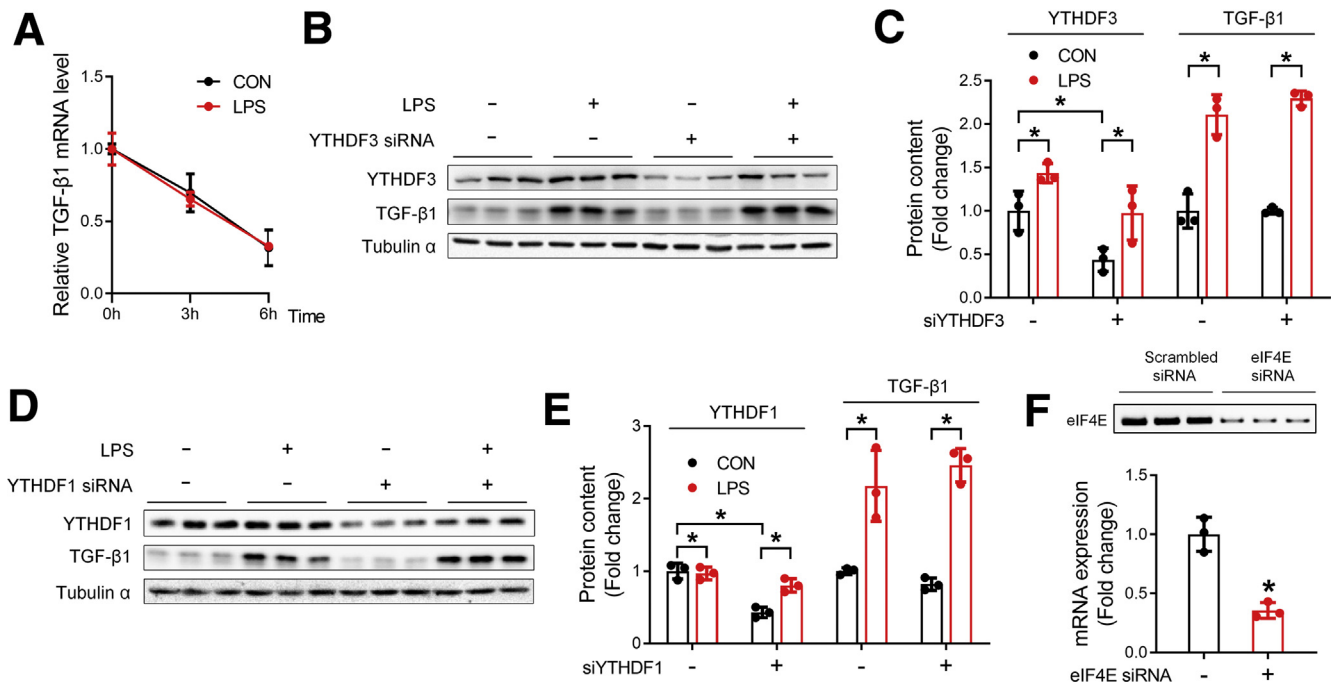


Figure 8. YTHDF1/YTHDF3 knockdown cannot inhibit the increase of TGF- β 1 content in LPS group. (A) Lifetime of TGF- β 1 mRNA in control and LPS-treated cells. Relative mRNA levels were quantified by qPCR; $n = 3$; mean \pm SD; Student's t test. (B, C) Protein content of YTHDF3 and TGF- β 1 were detected by Western blot when knockdown of YTHDF3 in LPS-treated cells; $n = 3$; mean \pm SD; 2-way analysis of variance followed by Tukey's test for multiple comparisons; $*P < .05$. (D, E) Protein content of YTHDF1 and TGF- β 1 were detected by Western blot when knockdown of YTHDF1 in LPS-treated cells; $n = 3$; mean \pm SD; 2-way analysis of variance followed by Tukey's test for multiple comparisons; $*P < .05$. (F) eIF4E siRNA efficiency were confirmed by qPCR and electrophoresis; $n = 3$; mean \pm SD; Student's t test; $*P < .05$.

regulation in LPS-activated KCs. Indeed, m⁶A modification was not detected in either IL-1 β or IL-6 mRNAs, and m⁶A modification in TNF- α mRNA was not responsive to LPS in KCs (data not shown). Such specificity of m⁶A action may be desired for targeting TGF- β 1 activation in fibrosis progression of nonalcoholic steatohepatitis.

In conclusion, m⁶A modification level is increased in the liver of HFD rats and LPS-activated KCs. METTL3/METTL14 knockdown inhibits KC and hepatic stellate cell activation by reducing TGF- β 1 content in an m⁶A-dependent manner. NF- κ B p65 transactivates both m⁶A methyltransferases METTL3 and METTL14 by directly binding to their promoters, thereby increasing the m⁶A modification in the TGF- β 1 mRNA 5'UTR to promote cap-independent translation. These findings shed new light on the m⁶A-mediated epigenetic regulation in the process of LPS-induced KC activation and implicate novel drug targets for the control of NASH to liver fibrosis progression.

Materials and Methods

Ethics Statement

All the experiments were approved by the Animal Ethics Committee of Nanjing Agricultural University. The sampling procedures followed the "Guidelines on Ethical Treatment of Experimental Animals" (2006) No. 398 set by the Ministry of Science and Technology, China.

Animals and Treatment

Male specific pathogen-free Sprague Dawley rats (6 weeks of age) were purchased from Beijing Vital River Laboratory Animal Technology (Beijing, China) and raised at the Animal Core Facility of Nanjing Medical University (Nanjing, China) at the temperature of $22 \pm 0.5^\circ\text{C}$, humidity of $50 \pm 5\%$, and a 12-hour light-dark cycle. After 1 week of acclimatization, the rats were randomly divided into 2 groups fed a control diet with 10% of energy from fat ($n = 8$) and a HFD with 45% of energy from fat ($n = 8$), respectively, for 16 weeks.

METTL14^{fllox/fllox} mice with floxed alleles were bred with Lyz2-Cre mice to generate myeloid lineage cell-specific METTL14 knockout (METTL14 cKO) mice that was used for functional validation in KCs.³⁰ Both strains of transgenic mice came from a C57BL/6J genetic background. At 8 weeks of age, METTL14 cKO and WT mice were challenged with LPS (Sigma-Aldrich, St. Louis, MO; L2880, single intraperitoneal injection at 5 mg/kg, $n = 3$) or CCl₄ (10%, Macklin, Shanghai, China; C805332, intraperitoneal injection at 5 mL/kg diluted with corn oil, twice per week for 4 weeks, $n = 3$). The corresponding control groups were treated with single intraperitoneal injection of saline ($n = 3$) or intraperitoneal injection of corn oil twice per week for 4 weeks ($n = 3$), respectively. Two hours after LPS injection and 4 weeks after CCl₄ treatment, METTL14 cKO and WT mice were etherized and the primary KCs were isolated from liver according to a previously published method.³¹

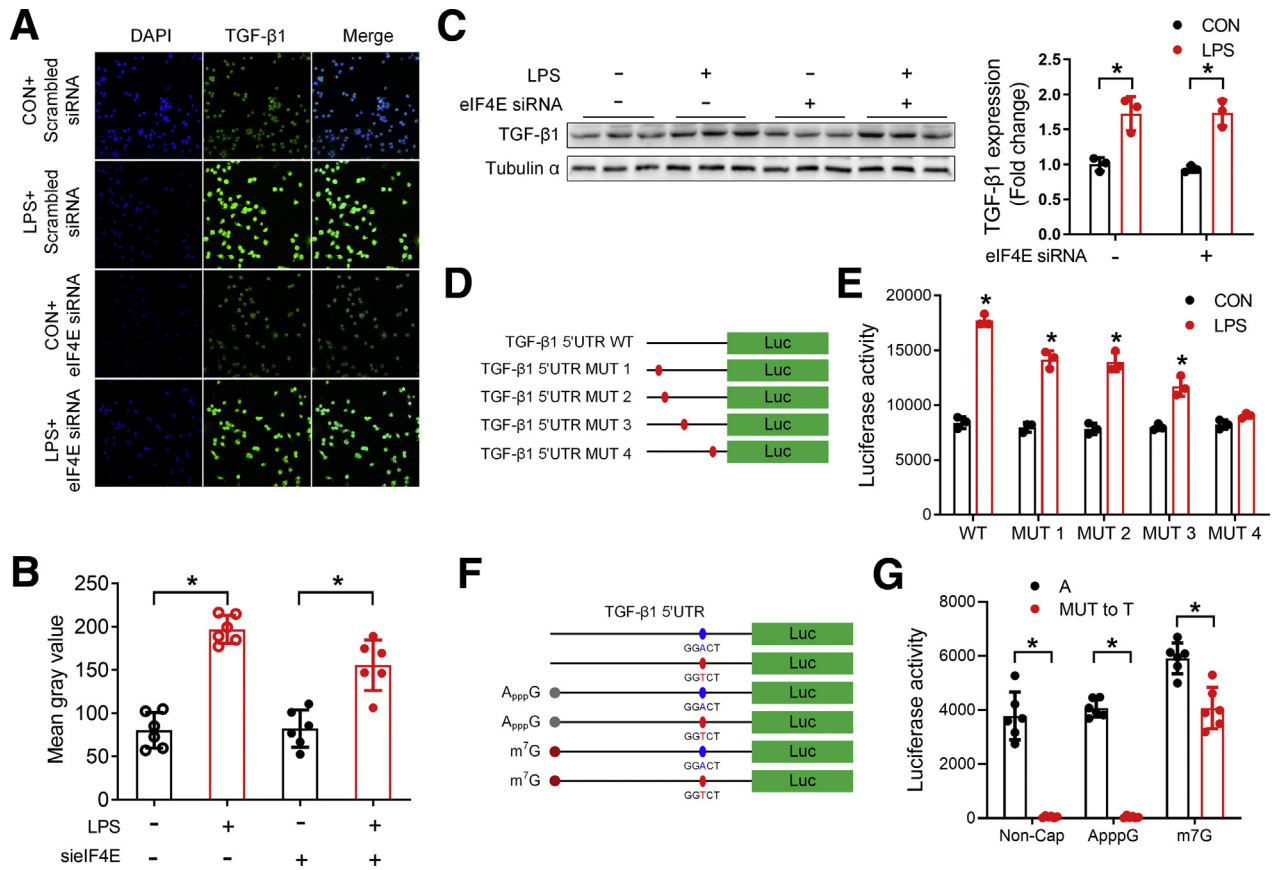


Figure 9. TGF-β1 5'UTR m⁶A promotes cap-independent translation. (A) eIF4E siRNA was transfected into with or without LPS-treated KCs, and TGF-β1 expression was measured by immunofluorescence; $n = 3$. DAPI was used for nuclear staining. Cells analyzed with a confocal laser scanning microscope (40 \times magnification) with Z-scan analysis. (B) Count the mean gray value by ImageJ software; mean \pm SD; 2-way analysis of variance followed by Tukey's test for multiple comparisons; $*P < .05$. (C) TGF-β1 expression was measured by Western blot; $n = 3$; mean \pm SD; 2-way analysis of variance followed by Tukey's test for multiple comparisons; $*P < .05$. (D) Schematic representation of mutated (GGACT to GGCCT, red dots) 5'UTR of pGL3-Basic vector to investigate the m⁶A roles on TGF-β1 expression. (E) Dual-luciferase activity of pGL3-Basic-5'UTR WT or pGL3-Basic-5'UTR MUT1/2/3/4 reporter were transfected into CON or LPS-treated KCs; $n = 3$; mean \pm SD; Student's t test; $*P < .05$. (F) Schematic representation of synthetic mRNAs containing TGF-β1 5'UTR and full-length firefly luciferase. Blue dots, normal m⁶A site (GGACT); red dots, mutated m⁶A site (GGACT to GGCCT). (G) Synthetic mRNAs were transfected and luciferase activity was detected in HEK293T cells; $n = 6$; mean \pm SD; 2-way analysis of variance followed by Tukey's test for multiple comparisons; $*P < .05$.

Serum Concentrations of Biochemical Parameters

The activities of aspartate aminotransferase (CH0103202) and alanine aminotransferase (CH0103213), which reflect liver injury, were measured in the serum with a biochemical automatic analyzer (Hitachi 7020; HITACHI, Tokyo, Japan) using commercial assay kits purchased from Maccara Biotechnology (Chengdu, China). The endotoxin (LPS) level in the serum was assayed using a Bioendo KT Endotoxin Test Kit from Xiamen Bioendo Technology (Xiamen, China) according to the manufacturer's protocol.

Cytokine Quantification

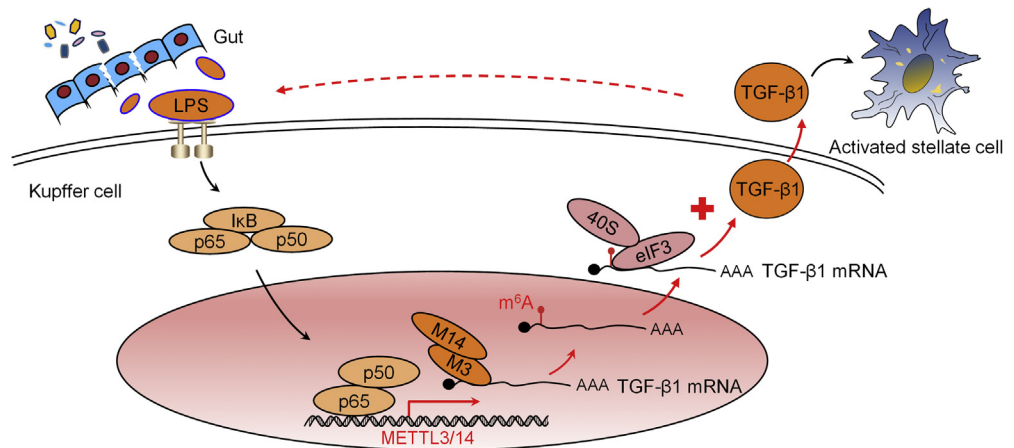
IL-1 β , IL-6, TNF- α , and TGF-β1 concentrations in the liver and in cell culture supernatant were quantified using enzyme-linked immunosorbent assay kits purchased from

Multisciences (Hangzhou, China) according to the manufacturer's instructions.

Isolation of Primary Kupffer Cells

Briefly, an etherized mouse was first perfused with calcium-free Hanks' balanced salt solution, followed by collagenase digestion. After digestion, the hepatocytes were released by mechanical dissociation of the lobes and underwent several steps of filtration with calcium containing Hanks' balanced salt solution and centrifugation at 50 g for 5 minutes. The supernatant containing nonparenchymal cells was loaded on a Percoll gradient (25% and 50%; Solarbio, Beijing, China) and centrifuged for 30 minutes at 2000 g at 4 $^{\circ}$ C. The interphase ring with enriched KCs was collected. The cells were then washed twice before RNA and protein extraction for subsequent analyses.

Figure 10. Proposed working model of the proposed mechanism in this study. The classic inflammatory NF- κ B pathway hijacks the m⁶A methyltransferases METTL3 and METTL14 to empower cap-independent translation of TGF- β 1, thus aggravating TGF- β 1-mediated stellate cell activation to promote the process of NASH to liver fibrosis transition.



Cell Culture and Treatment

Mouse KC lines (BeNa Culture Collection, Beijing, China; BNCC340733) were cultured in RPMI 1640 (Wisent, Saint-Jean-Baptiste, Quebec, Canada) containing 10% fetal bovine serum (Gibco, Gaithersburg, MD), and 1% penicillin/streptomycin (Gibco) at 37°C under 5% CO₂. Cells were cultured to 80% confluence and then treated with 1 μg/mL LPS (L2880; Sigma-Aldrich) for 12 hours.

Histopathology and Immunofluorescence

Fresh liver tissue was fixed with 4% paraformaldehyde and paraffin embedded, and then the sections (4 μm) of liver were stained with hematoxylin and eosin, Sirius Red, and Masson. The red area in Sirius staining, considered the fibrotic area, was assessed by computer-assisted image analysis with ImageJ software V1.8.0.112 (National Institutes of Health, Bethesda, MD). Immunofluorescence was used for checking the expression of CD68 (ab955; Abcam, Cambridge, MA; diluted 1:500), Collagen I (BA0325; Boster Biological Technology, Wuhan, China; diluted 1:100) and TGF- β 1 (bsm33345; Bioss, Beijing, China; diluted 1:100). DAPI (Molecular Probes, Eugene, OR) was used to label cell nuclei.

RNA Isolation, Real-Time qPCR

Total RNA was isolated from 30-mg liver samples by using TRIzol Reagent (3101; Shanghai Pufei Biotechnology, Shanghai, China), and 1 μg of RNA was reverse-transcribed into complementary DNA by using a HiScript II Reverse Transcriptase kit (R233-01; Vazyme, Nanjing, China) according to the manufacturer's protocol. A total of 2 μL of diluted complementary DNA (1:20, v:v) was used for real-time qPCR by using a Mx3000P Real-Time PCR System (Stratagene, San Diego, CA). All primers (Table 1) were synthesized by Genewiz Biotech (Suzhou, China). GAPDH was chosen as a reference gene and was not affected by treatment. Data were analyzed by using the method of 2^{-ΔΔCT}.

Protein Extraction and Western Blot Assay

The protein concentrations were measured by BCA Protein Assay kit (No.23225; Thermo Fisher Scientific, Waltham, MA) according to the manufacturer's instructions. A total of 40-μg proteins were used for electrophoresis on a 10% and 15% sodium dodecyl sulfate polyacrylamide gel electrophoresis gel and transferred onto a nitrocellulose membrane. The primary antibodies used for Western blot analysis are listed in Table 2. Tubulin- α and β -actin were selected as internal controls. Images were captured by VersaDoc 4000MP system (Bio-Rad, Hercules, CA) and the band density was analyzed with Quantity One software (Bio-Rad).

ChIP Assay

Cells were crosslinked in 1% formaldehyde and quenched by addition of 125 mM glycine, scraped, and collected by centrifugation, then washed twice with cold phosphate-buffered saline. Cells were lysed from 1 plate (10 cm in diameter) with 1-mL sodium dodecyl sulfate lysis buffer containing protease inhibitor cocktail (11697498001; Roche, Indianapolis, IN), by resuspension the pellet and pipetting up and down several times in a microcentrifuge tube. Crude chromatin preparations were sonicated on ice to yield DNA fragments of 150–300 bp in length and pre-cleared with salmon sperm DNA-treated protein A/G agarose beads (40 μL, 50% slurry, sc-2003; Santa Cruz Biotechnology, CA). The mixture of pre-cleared chromatin preparations and 2 μg of primary antibody p65 (8242; Cell Signaling Technology, Danvers, MA) were incubated overnight at 4°C. A negative control was included with normal IgG. Protein A/G agarose beads were added to capture the immunoprecipitated chromatin complexes. Finally, DNA fragments were released from the immunoprecipitated complexes by reverse cross-linking at 65°C for 1 hour, and quantitative real-time PCR was used to quantify the fragments of target gene promoters with specific primers (Table 1) using purified immunoprecipitated DNA as the template.

Table 1. Nucleotide Sequences of Primers

Target	Primer Sequence (5' to 3')		Used for
IL-1 β	F: AATGCCACCTTTTGACAGTGATG	R: GGAAGGTCCACGGGAAAGAC	qPCR
IL-6	F: GGAAGGTCCACGGGAAAGAC	R: GGAAGGTCCACGGGAAAGAC	qPCR
TNF- α	F: AGGCACTCCCCAAAAGATG	R: CCACTTGGTGGTTTGTGAGTG	qPCR
Collagen I	F: AGCACGTCTGGTTTGGAGAG	R: GCTGTAGGTGAAGCGACTGT	qPCR
TGF- β 1	F: ACTGGAGTTGTACGGCAGTG	R: GGATCCACTTCCAACCCAGG	qPCR
TGF- β 2	F: GTCACAACAGGGGAAGACCC	R: GTGCTGAGTCTGTCACTCCATA	qPCR
TGF- β 3	F: GGGAGGAAGGCTCACTTTACAA	R: CAAGACCCGGAAGAGCTCAA	qPCR
α -SMA	F: AAGCGAGGTATCCTGACCCT	R: GATGTCGCGCACAATCTCAC	qPCR
GAPDH	F: GGAGAGTGTTCCTCGTCCC	R: ACTGTGCCGTTGAATTTGCC	qPCR
METTL3-Promoter	F: ATCCTTGGGGACAGTGAACCT	R: CGATTGTGAGACGACGTTGC	ChIP-PCR
METTL14-Promoter 1	F: TCTAGTCCCGGCAGTCATAA	R: AGAGCAAATTTTCAGGGCAGC	ChIP-PCR
METTL14-Promoter 2	F: GCGATCCAGTCCCTCACAA	R: CTGAACAGGAAGTCCCGCC	ChIP-PCR
TNF- α	F: CCTCTCTACCTTGTGGCC	R: AGGTGCCTGAGAATGTGG	MeRIP-PCR
SOCS3	F: TGGCACAAGCACAAAAT	R: CCCTTACACACCCTTTT	MeRIP-PCR
TGF- β 1 5'UTR Motif 4	F: GCTGCTTTCTCCCTCAACCT	R: CTGCAGGGCTTGTGGGG	MeRIP-PCR

α -SMA, α -smooth muscle actin; ChIP, chromatin immunoprecipitation; IL, interleukin; MeRIP, methylated RNA immunoprecipitation; qPCR, quantitative polymerase chain reaction; PCR, polymerase chain reaction; TGF-B, transforming growth factor β ; TNF- α , tumor necrosis factor α ; UTR, untranslated region.

Quantitative Analysis of m⁶A Level Using Liquid Chromatography With Tandem Mass Spectrometry

mRNA was purified from total RNA using Dynabeads mRNA DIRECT kit (61006, Thermo Fisher Scientific) according to the manufacturer's instructions. Briefly, 25 μ L Reaction Buffer (20 mM of ZnCl₂, 100 mM of NaCl) and 1 μ L Nuclease P1 (N8630-1VI; Sigma-Aldrich) were added to 200 ng of purified mRNA and incubated at 37°C for 2 hours, followed by the addition of NH₄HCO₃ (1 M, 3 μ L) and alkaline phosphatase (0.5 U, EF0651; Invitrogen, Carlsbad, CA) for 2 hours at 37°C. The digestion mixture was diluted to 1 mL using deionized water and centrifuged at 10,000 rpm for 5 minutes to

remove any solid material. The digestion mixture was then filtered with 0.22 μ M Millipore membrane (MilliporeSigma, Burlington, VT), and 5 μ L of this solution was injected into the liquid chromatography with tandem mass spectrometry system. A and m⁶A were later separated by UPLC-ESI-QQQ on a C18 column (Rapid Resolution HT, 50 mm \times 2.1 mm I.D, 1.8 μ m; Agilent, Santa Clara, CA). Formic acid in water (0.1%, v/v, solvent A) and formic acid in methanol (0.1%, v/v, solvent B) were employed as the mobile phase. The mass spectrometry detection was performed under positive electrospray ionization mode, by which the product ion scans of the protonated A at m/z (268 \rightarrow 136) and m⁶A at m/z (282 \rightarrow 150) were acquired. The quantification

Table 2. The Primary Antibodies Used for Western Blot Analysis

Primary Antibody	Company	Catalog No.	Dilution
METTL3	Abcam	AB98009	1:1000
METTL14	Abcam	AB98116	1:1000
FTO	Abcam	AB77547	1:1000
Collagen I	Boster Biological Technology	BA0325	1:500
TGF- β 1	Proteintech	21898-1-AP	1:1000
α -SMA	Zen bioscience	252157	1:500
IKK γ	Bioworld	BS6772	1:1000
p-IKK α/β	Bioworld	BS5083	1:1000
p-p65	Cell Signaling Technology	3033	1:1000
Tubulin- α	Bioworld	BS1699	1:5000
β -actin	Bioworld	BS6007M	1:5000

α -SMA, α -smooth muscle actin; FTO, fat mass and obesity-associated protein; p-p65, phosphorylated p65; TGF- β 1, transforming growth factor β 1.

Table 3. Nucleotide Sequences of SELECT Method

Target	Sequences (5' to 3')
TGF- β 1 5'UTR Motif 4 X site	Up probe: tagccagtagcgtgccaaggaaggtaggtgatag
	Down probe: CCTGAATAATTTGAGGTTGAcagaggctgagtcgctgcat
TGF- β 1 5'UTR Motif 4 N site (Internal Control)	Up probe: tagccagtagcgtgaaaggtaggtgatagtcctga
	Down probe: TAATTTGAGGTTGAGGGAGAcagaggctgagtcgctgcat
qPCR	Forward prime: ATGCAGCGACTCAGCCTCTG
	Reverse prime: TAGCCAGTACCGTAGTGCGTG

qPCR, quantitative polymerase chain reaction; UTR, untranslated region.

was carried out using a standard curve generated from A and m⁶A standards (0.1–10 nM for m⁶A, 50–2000 nM for A) ran during the same batch of the samples. The m⁶A level was calculated as the ratio of m⁶A to A.

m⁶A-Seq and Relative Data Analysis

The m⁶A-sequencing and data analysis were performed by RiboBio (Guangzhou, China). For data analysis, read sequences were filtered by the FASTQC and then aligned to the mouse genome (National Center for Biotechnology Information build 38/mm10) using BWA mem v 0.7.12 (<http://bio-bwa.sourceforge.net>). MACS version 2.1.0.20151222 (<https://github.com/jsh58/MACS>) was used for peak detection. A q-value threshold of enrichment of 0.05 was used for all data sets. MEME version 4.11.1 (<https://meme-suite.org/meme>) and DREME version 4.11.1 (<http://meme.nbcr.net>) were used to detect the sequence motif, after which, Tomtom software (<https://meme-suite.org/meme/tools/tomtom>) was used to annotate the motifs. Integrative Genomics Viewer (<https://software.broadinstitute.org/software/igv/>) were used to visualize the distributions of the m⁶A peaks.

MeRIP-qPCR for Detection of m⁶A

Total RNA was isolated and chemically fragmented (0.1 M Tris-HCl, pH = 7.0; 0.1 M EDTA, pH = 8.0) to approximately 200 nt in size, ethanol-precipitated and purified using the EasyPure RNA Purification Kit (ER701-01; TransGen, Beijing, China). 40 μ g fragmented total RNA was precleared with protein A/G agarose beads (40 μ L, sc-2003;

Santa Cruz Biotechnology) supplemented with 40U RNase inhibitor overnight at 4°C. The mixture and 2 μ g m⁶A antibody (ab151230; Abcam) were incubated overnight at 4°C. A negative control was included with normal IgG (2729S; Cell Signaling Technology). Protein A/G agarose beads were added to capture the immunoprecipitated complexes. RNA was eluted from the beads by incubation in 300 μ L of elution buffer (5 mM Tris-HCl, pH = 7.4; 1 mM EDTA, pH = 8.0 and 0.05% sodium dodecyl sulfate) with 20 μ g of proteinase K for 1 hour at 60°C. Following phenol extraction and ethanol precipitation, the input and m⁶A-enriched RNA were reversely transcribed with random hexamers, and the enrichment was determined by qPCR. The primers used for detection for m⁶A-enriched gene mRNA were shown in Table 1.

SELECT for Detection of m⁶A

The methylation status was confirmed using SELECT.¹⁵ Briefly, 5 μ g total RNA was incubated with 40 nM Up Primer, 40 nM Down Primer, and 5 μ M dNTP in 17 μ L 1 \times CutSmart buffer (50 mM KAc, 20 mM Tris-HAc, 10 mM MgAc₂, 100 μ g/mL bovine serum albumin), and annealed under the programs below: 90°C (1 minutes), 80°C (1 minutes), 70°C (1 minutes), 60°C (1 minutes), 50°C (1 minutes), and 40°C (6 minutes). Next, 17- μ L annealing products were incubated with a 3 μ L of enzyme mixture containing 0.01 U Bst 2.0 DNA polymerase (M0537I; NEB, USA), 0.5 U SplintR ligase (M0375I; New England Biolabs, Ipswich, MA), and 10 nmol adenosine triphosphate (P0756S; New England Biolabs). The final 20- μ L reaction mixture was incubated at 40°C for 20 minutes, denatured at 80°C for 20 minutes, and kept at 4°C. qPCR analysis was carried out as described previously and was run under the following conditions: 95°C, 5 minutes; 95°C, 10 seconds; and 60°C, 45 seconds for 40 cycles. The SELECT products of indicated site were normalized to the RNA abundance of indicated transcript bearing this site. Primers used in SELECT assay are listed in the Table 3.

Plasmids and Transfection

About 2000 bp of METTL3/METTL14 promoter fragments were cloned into a pGL3-basic vector (Promega, Madison, WI) between XhoI and HindIII sites. NF- κ B binding site-deleted fragments were generated using this plasmid

Table 4. Nucleotide Sequences of siRNA

Target	Source
METTL3	siB171201025317-1-5, RiboBio
METTL14	siG14311110202-1-5, RiboBio
YTHDF1	siG151229103944-1-5, RiboBio
YTHDF3	siG160425113657-1-5, RiboBio
eIF4E	siB1904240322029471, RiboBio
Negative control	siN0000001-1-5, RiboBio

siRNA, small interfering RNA.

Table 5. Nucleotide Sequences of Plasmid Construction

Target	Primer Sequences (5' to 3')
pGL3-METTL3 Promoter	F: ggatctccagagatctcgagCTGCTCTCTTCTCCCTCCC R: ctgccgttcgacgataagcctGGCGAACCAGCCGGACGT
pGL3-METTL14 Promoter	F: ggatctccagagatctcgagCATATATAAACTGTGCAAGAGGAAAATT R: ctgccgttcgacgataagcctTTAAAGTCTTTCCTGAAGGGTTAGG
pGL3-TGF- β 1 5'UTR	F: ggatctccagagatctcgagGCTGGGGCGCACCCCTTG R: ctgccgttcgacgataagcctGGGGGAGGCGGCGCCCCA
UTR, untranslated region.	

DNA as a template. The primers used for PCR amplification are listed in Table 1. Cells were transfected at 50%–70% confluence with siRNA (RiboBio, Guangzhou, China), sequences are listed in the Table 4. The complete TGF- β 1 mRNA 5'UTR was obtained by PCR from mice DNA. Based on the results of m⁶A-seq, the m⁶A site was predicted in sequence-based m⁶A modification site predictor (<http://www.cuilab.cn/sramp>) for the sequence between 25687587 and 25687822 nt, and a high-confidence site A was obtained, which was mutated to T (named TGF- β 1 5'UTR MUT4), 3 other A, which, matching RRACH, were mutated to T as well (named TGF- β 1 5'UTR MUT1, 2, and 3, respectively). The 4 sequences were cloned into pGL3-basic vector between XhoI and HindIII sites. For transfection, cells were seeded into a 6-well plate and transfected with plasmids using Lipofectamine 2000 (Invitrogen), following the manufacturer's instructions. Primers used in plasmid construction are listed in Table 5.

RNA Decay Assay

To evaluate the RNA stability, RNA decay assay was conducted. KCs were cultured in 6-well plates followed by the treatment with or without LPS. Then actinomycin D (HY-17559, MCE, NJ) was added into each well to a final concentration of 5 μ g/mL. Cells were collected after 0, 3, 6 hours, respectively. Total RNA was isolated and subjected to reverse-transcription qPCR subsequently to quantify the relative abundance of TGF- β 1 mRNA (relative to 0 hours).

In Vitro Transcription

Plasmids containing the wide-type and m⁶A site mutant 5'UTR sequences (25687587–25687822) of mouse TGF- β 1 and full-length firefly luciferase were used as templates. Transcripts with noncap, nonfunctional (A_{ppp}G) cap (S1407S; New England Biolabs), and normal (m⁷G) cap (S1404S; New England Biolabs) were generated using the T7 High Yield Transcription Kit (TR101-01; Vazyme, Nanjing, China). All mRNA products were purified using the EasyPure RNA Purification Kit (ER701-01; TransGen) according to the manufacturer's instruction.

Real-Time Luciferase Assay

HEK293T cells were seeded into a 6-well plate and transfected with in vitro synthesized mRNA containing

the luciferase gene by Lipofectamine 2000 (Invitrogen). Luciferase substrate D-Luciferin sodium salt (1 mM, HY-12591; MCE) was added into the culture medium immediately after transfection. Luciferase activity was detected on the GloMax 96 Microplate Luminometer (Promega).

Statistical Analysis

All data are presented as mean \pm SD. Most experiments were repeated at least twice. All bioinformatic analyses were conducted using duplicate biological samples. The differences between groups were analyzed using Student's *t* test or 2-way analysis of variance followed by Tukey's test for multiple comparisons with SPSS 20.0 (IBM, Armonk, NY). The differences were considered statistically significant when *P* < .05.

References

1. Dooley S, ten Dijke P. TGF- β in progression of liver disease. *Cell Tissue Res* 2012;347:245–256.
2. Tsuchida T, Friedman SL. Mechanisms of hepatic stellate cell activation. *Nat Rev Gastroenterol Hepatol* 2017; 14:397–411.
3. Azzariti A, Mancarella S, Porcelli L, Quatralo AE, Caligiuri A, Lupo L, Dituri F, Giannelli G. Hepatic stellate cells induce hepatocellular carcinoma cell resistance to sorafenib through the laminin-332/alpha3 integrin axis recovery of focal adhesion kinase ubiquitination. *Hepatology* 2016;64:2103–2117.
4. Kim KA, Gu W, Lee IA, Joh EH, Kim DH. High fat diet-induced gut microbiota exacerbates inflammation and obesity in mice via the TLR4 signaling pathway. *PLoS One* 2012;7:e47713.
5. Cani PD, Bibiloni R, Knauf C, Waget A, Neyrinck AM, Delzenne NM, Burcelin R. Changes in gut microbiota control metabolic endotoxemia-induced inflammation in high-fat diet-induced obesity and diabetes in mice. *Diabetes* 2008;57:1470–1481.
6. Wiest R, Albillos A, Trauner M, Bajaj JS, Jalan R. Targeting the gut-liver axis in liver disease. *J Hepatol* 2017; 67:1084–1103.
7. Zaccara S, Ries RJ, Jaffrey SR. Reading, writing and erasing mRNA methylation. *Nat Rev Mol Cell Biol* 2019; 20:608–624.
8. Garcias Morales D, Reyes JL. A birds'-eye view of the activity and specificity of the mRNA m⁶A methyltransferase complex. *WIREs RNA* 2020 Jun 17 [E-pub ahead of print].

9. Shulman Z, Stern-Ginossar N. The RNA modification N-methyladenosine as a novel regulator of the immune system. *Nat Immunol* 2020;21:501–512.
10. Li HB, Tong J, Zhu S, Batista PJ, Duffy EE, Zhao J, Bailis W, Cao G, Kroehling L, Chen Y, Wang G, Broughton JP, Chen YG, Kluger Y, Simon MD, Chang HY, Yin Z, Flavell RA. m(6)A mRNA methylation controls T cell homeostasis by targeting the IL-7/STAT5/SOCS pathways. *Nature* 2017;548:338–342.
11. Wang H, Hu X, Huang M, Liu J, Gu Y, Ma L, Zhou Q, Cao X. Mettl3-mediated mRNA m(6)A methylation promotes dendritic cell activation. *Nat Commun* 2019; 10:1898.
12. Feng Z, Li Q, Meng R, Yi B, Xu Q. METTL3 regulates alternative splicing of MyD88 upon the lipopolysaccharide-induced inflammatory response in human dental pulp cells. *J Cell Mol Med* 2018; 22:2558–2568.
13. Ma JZ, Yang F, Zhou CC, Liu F, Yuan JH, Wang F, Wang TT, Xu QG, Zhou WP, Sun SH. METTL14 suppresses the metastatic potential of hepatocellular carcinoma by modulating N(6) -methyladenosine-dependent primary MicroRNA processing. *Hepatology* 2017; 65:529–543.
14. Chen M, Wei L, Law CT, Tsang FH, Shen J, Cheng CL, Tsang LH, Ho DW, Chiu DK, Lee JM, Wong CC, Ng IO, Wong CM. RNA N6-methyladenosine methyltransferase-like 3 promotes liver cancer progression through YTHDF2-dependent posttranscriptional silencing of SOCS2. *Hepatology* 2018;67:2254–2270.
15. Xiao Y, Wang Y, Tang Q, Wei L, Zhang X, Jia G. An elongation- and ligation-based qPCR amplification method for the radiolabeling-free detection of locus-specific N(6) -methyladenosine modification. *Angew Chem Int Ed Engl* 2018;57:15995–16000.
16. Dewidar B, Meyer C, Dooley S, Meindl-Beinker AN. TGF- β in hepatic stellate cell activation and liver fibrogenesis updated 2019. *Cells* 2019;8:1419.
17. Xiao YQ, Freire-de-Lima CG, Schiemann WP, Bratton DL, Vandivier RW, Henson PM. Transcriptional and translational regulation of TGF-beta production in response to apoptotic cells. *J Immunol* 2008; 181:3575–3585.
18. Meyer KD, Patil DP, Zhou J, Zinoviev A, Skabkin MA, Elemento O, Pestova TV, Qian S-B, Jaffrey SR. 5' UTR m(6)A promotes Cap-independent translation. *Cell* 2015; 163:999–1010.
19. Zhou J, Wan J, Gao X, Zhang X, Jaffrey SR, Qian S-B. Dynamic m(6)A mRNA methylation directs translational control of heat shock response. *Nature* 2015; 526:591–594.
20. Xiang Y, Laurent B, Hsu C-H, Nachtergaele S, Lu Z, Sheng W, Xu C, Chen H, Ouyang J, Wang S, Ling D, Hsu P-H, Zou L, Jambhekar A, He C, Shi Y. RNA mA methylation regulates the ultraviolet-induced DNA damage response. *Nature* 2017;543:573–576.
21. Anders M, Chelysheva I, Goebel I, Trenkner T, Zhou J, Mao Y, Verzini S, Qian S-B, Ignatova Z. Dynamic mA methylation facilitates mRNA triaging to stress granules. *Life Sci Alliance* 2018;1:e201800113.
22. Wang X, Lu Z, Gomez A, Hon GC, Yue Y, Han D, Fu Y, Parisien M, Dai Q, Jia G, Ren B, Pan T, He C. N6-methyladenosine-dependent regulation of messenger RNA stability. *Nature* 2014;505:117–120.
23. Huang H, Weng H, Sun W, Qin X, Shi H, Wu H, Zhao BS, Mesquita A, Liu C, Yuan CL, Hu YC, Huttelmaier S, Skibbe JR, Su R, Deng X, Dong L, Sun M, Li C, Nachtergaele S, Wang Y, Hu C, Ferchen K, Greis KD, Jiang X, Wei M, Qu L, Guan JL, He C, Yang J, Chen J. Recognition of RNA N(6)-methyladenosine by IGF2BP proteins enhances mRNA stability and translation. *Nat Cell Biol* 2018;20:285–295.
24. Li A, Chen YS, Ping XL, Yang X, Xiao W, Yang Y, Sun HY, Zhu Q, Baidya P, Wang X, Bhattarai DP, Zhao YL, Sun BF, Yang YG. Cytoplasmic m(6)A reader YTHDF3 promotes mRNA translation. *Cell Res* 2017; 27:444–447.
25. Wang X, Zhao BS, Roundtree IA, Lu Z, Han D, Ma H, Weng X, Chen K, Shi H, He C. N(6)-methyladenosine modulates messenger RNA translation efficiency. *Cell* 2015;161:1388–1399.
26. Tisoncik JR, Korth MJ, Simmons CP, Farrar J, Martin TR, Katze MG. Into the eye of the cytokine storm. *Microbiol Mol Biol Rev* 2012;76:16–32.
27. Bird L. Calming the cytokine storm. *Nat Rev Immunol* 2018;18:417.
28. Schuler GS, Grom AA. Pathogenesis of macrophage activation syndrome and potential for cytokine-directed therapies. *Annu. Rev. Med* 2015;66:145–159.
29. Tong AJ, Liu X, Thomas BJ, Lissner MM, Baker MR, Senogolage MD, Allred AL, Barish GD, Smale ST. A stringent systems approach uncovers gene-specific mechanisms regulating inflammation. *Cell* 2016; 165:165–179.
30. Beattie L, Sawtell A, Mann J, Frame TCM, Teal B, de Labastida Rivera F, Brown N, Walwyn-Brown K, Moore JWW, MacDonald S, Lim EK, Dalton JE, Engwerda CR, MacDonald KP, Kaye PM. Bone marrow-derived and resident liver macrophages display unique transcriptomic signatures but similar biological functions. *J Hepatol* 2016;65:758–768.
31. Aparicio-Vergara M, Tencerova M, Morgantini C, Barreby E, Aouadi M. Isolation of Kupffer cells and hepatocytes from a single mouse liver. *Methods Mol Biol* 2017;1639:161–171.

Received January 19, 2021. Accepted May 7, 2021.

Correspondence

Address correspondence to Ruqian Zhao, PhD, Director of Key Laboratory of Animal Physiology & Biochemistry, College of Veterinary Medicine, Nanjing Agricultural University, Nanjing 210095, P. R. China. e-mail: zhaoruqian@njau.edu.cn; fax: 025-4442173.

Acknowledgments

The authors thank Prof. Jian Peng (Huazhong Agricultural University) for providing advice about liquid chromatography with tandem mass spectrometry; Dr Tongxing Song and Yanan Wang (Huazhong Agricultural University) for helping with liquid chromatography with tandem mass spectrometry analysis.

CRedit Authorship Contributions

Yue Feng (Investigation: Lead; Methodology: Lead; Writing – original draft: Equal)

Haibo Dong (Conceptualization: Supporting; Investigation: Equal; Methodology: Supporting; Validation: Equal)

Bo Sun (Methodology: Equal; Resources: Equal)

Yun Hu (Conceptualization: Supporting; Investigation: Supporting; Methodology: Supporting)

Yang Yang (Data curation: Supporting; Methodology: Supporting; Validation: Supporting)

Yimin Jia (Software: Supporting; Validation: Supporting; Visualization: Supporting)

Longfei Jia (Data curation: Supporting; Methodology: Equal)

Xiang Zhong (Resources: Supporting; Providing the myeloid lineage cell-specific Mett14 knockout mouse model: Supporting)

Ruqian Zhao (Conceptualization: Lead; Data curation: Lead; Funding acquisition: Lead; Project administration: Lead; Supervision: Lead; Writing – original draft: Lead)

Conflicts of interest

The authors disclose no conflicts.

Funding

This work was supported by the National Natural Science Foundation of China (31972638, 31672512), the National Key Research and Development Program of China (2016YFD0500502), the Fundamental Research Funds for the Central Universities (KYZ201212), the Priority Academic Program Development of Jiangsu Higher Education Institutions, and the Jiangsu Collaborative Innovation Centre of Meat Production and Processing, Quality and Safety Control.